THREE-DIMENSIONAL COMPUTATION OF NATURAL CONVECTION IN THE PRESENCE OF MAGNETIC FIELD (CUBIC ENCLOSURE)

[1*] Kherief Nacereddine Mohamed, [2]Farid Berrahil and [2]Kamel Talbi
[1]Asma DEMBRI, [1]Mahmoud BENSACI[2]
[1]Normal High School of Technology Education ENSET-azzaba Skikda (Algeria).
[2]Department of Mechanical Engineering Mentouri University Constantine(Algeria).
* E-mail: Kherief2006.yahoo.fr

ABSTRACT

Buoyancy-driven magneto hydrodynamic flow in a liquid-metal filled cubic enclosure is investigated by three dimensional numerical simulations. The enclosure is heated and cooled along two opposite vertical walls, all other walls being adiabatic. A uniform magnetic field is applied orthogonally to the gravity vector and to the temperature gradient (i.e., parallel to the isothermal walls). The Prandtl number is = 0.019 (characteristic of Galium); the Rayleigh number is made to vary from 10^3 to 10^7, the Hartmann number between 30 to 120 and the electrical conductance of the walls between 0 and 1. The Navier–Stokes equations, for the electrical potential, are solved by a finite volume method using the CFD package CFX-4 with some necessary adaptations. Steady-state conditions are assumed. In all cases, a three-dimensional flow with complex secondary motions and a complex current pattern is established. The results show that the dynamic and temperature fields are strongly affected by variations of the magnetic field intensity and the angle of inclination.

Numerical simulations are carried out considering different combinations of Grashof and Hartmann numbers to study their effects on the streamlines, the isotherms and the Nusselt number. Wall electrical conductivity enhances damping by changing the distribution of the induced electric current to one which augments the magnitude of the Lorentz force.

Keywords: *Natural convection, Magnetic field, Cavity, Liquid metal, finite-volume, Lorentz force, three dimensional*

Introduction and previous work

Within the separated-cooled concept for the liquid metal breeder blanket of a power fusion reactor [1], the problem arises of understanding and characterizing buoyant flows in a low Prandtl number fluid under the influence of a strong magnetic field.

In this a crucible of molten material is slowly drawn from a furnace and solidification takes place. This technique is of significant practical importance in the growth of high-quality materials for optoelectronic applications as reviewed by Hill [2]. The industrial process may involve dendrite growth and the distribution of dopants and is thus a complicated problem. However, insights can be gained from studying the basic fluid dynamics that results from the differential heating of the sample since other processes are strongly influenced by the induced motion. For small temperature differences, the convection is steady and primarily consists of a large, single circulation. The bulk flow in a confined cavity evolves considerably for larger values of the driving force, as the interaction between the different regions of flow becomes significant. Thus, the mechanisms underlying the transitions to time-dependent and eventually turbulent flow are often complex. We refer to the review article by Muller & Ostrogorsky[3] for a discussion of convective effects in crystal growth. Our model Bridgman configuration consists of a rectangular, insulated enclosure of square cross-section where the ends are conducting. It contains liquid gallium and is heated and cooled in a controlled way at the two opposite ends. A schematic diagram of the geometry is presented in figure 1. We have chosen to investigate this relatively narrow configuration because of its practical relevance and we find that cross-flows are important since the onset of time dependence is essentially different to that studied in two-dimensional models With the application of an external magnetic field, it is possible to act on the flows without any physical contact, and thus to remove the fluctuations to control heat and mass transfers, in order to improve the quality of the crystal. For this purpose, the damping magnetic to control the flow induced by a temperature variation was used in several industrials applications. Tagawa and Ozoe [4] numerically studied three-dimensional natural convection of a liquid metal in a cubic enclosure, under the action of a magnetic field applied, according to the three main directions. Benhadid and Henry [5] studied the effect of a magnetic field on the flow of liquid metal in a parallelepiped cavity, using a spectral numerical method. Bessaih et al. [6] numerically examined the effect of the electric conductivity of the walls and the direction of the magnetic field on the flow of Gallium. Their results show a considerable reduction in the intensity of the convection when the magnetic field increases. Kherief N M. and al [7] obtained numerical solutions for the velocity and temperature fields inside the enclosure, to determine the effects of the magnetic field strength and direction, the inclination of the enclosure on the transport phenomena. The results show that the dynamic and temperature fields are strongly affected by variations of the magnetic field intensity and the angle of inclination. Numerical simulations have been carried out considering different combinations of Grashof and Hartmann numbers. Kherief N M. et al [8]. Steady, laminar, natural-convection flow in the presence of a magnetic field in an inclined rectangular enclosure heated from one side and cooled from the adjacent side was considered. The governing equations were solved numerically for the stream function, vorticity and temperature using the finite-volume method for various Grashof and

Hartmann numbers and inclination angles and magnetic field directions. The results show that the orientation and the strength and direction of the magnetic field have significant effects on the flow and temperature fields. Counterclockwise inclination induces the formation of multiple eddies inside the enclosure significantly affecting the temperature field. Circulation inside the enclosure and therefore the convection becomes stronger as the Grashof number increases while the magnetic field suppresses the convective flow and the heat transfer rate.

The aim of the present work is to examine in detail the effect of a magnetic field on natural convection and heat transfer in a three-dimensional cavity filled with an electrically conducting fluid. The applied magnetic field is assumed to be parallel to gravity. For many fluids used in the laboratory, the conductivity is usually small and hence the magnetic Reynolds number is very small. Therefore, we assume that the induced magnetic field produced by the motion of the electrically conducting fluid is negligible compared to the applied magnetic field B. Then the electromagnetic retarding force and the buoyancy force terms appear in the horizontal and vertical momentum equations respectively with a result that a boundary layer type of analysis is not applicable. Thus the equations are not amenable to analytical treatment. In the present paper we, therefore, solve the problem numerically using an implicit finite difference scheme which is computationally stable. The effect of various controlling parameters on fluid flow and heat transfer are examined.

NOMENCLATURE

A aspect ratio
B magnetic field [T]
B_0 uniform magnetic flux density
e_B unitary vector of the direction of B
Fx Lorentz force in the x-direction
Fy Lorentz force in the y-direction
Fz Lorentz force in the z-direction
g gravitational acceleration, $m.s^{-2}$
Gr Grashof number $= g\,\beta\left(T_H - T_C\right)\,H^3/\upsilon^2$
H height of the cavity, m
Ha Hartmann number $= B_0 H\sqrt{\sigma/\rho\upsilon}$
L length of the enclosure, m
J_x electric current in the x-direction, $A.m^{-2}$
J_y electric current in the y-direction, $A.m^{-2}$
J_z electric current in the z-direction, $A.m^{-2}$
δ_H dimensionless thickness Hartmann layer, $=Ha^{-1}$
δ_S dimensionless thickness side layer, $=Ha^{-1/2}$
Nu average Nusselt number
Nx nodes number in the x-direction
Ny nodes number in the y-direction
Nz nodes number in the z-direction
p pressure, $N.m^{-2}$
Pr Prandtl number $=\upsilon/\alpha$
Ra Rayleigh number
R_m Reynolds magnétic number
T temperature, K
T_H hot temperature [K]
T_C cold temperature [K]
u velocity in the x-direction, $m.s^{-1}$
U dimensionless velocity in the x-direction,
v velocity in the y-direction, $m.s^{-1}$
V dimensionless velocity in the y-direction
w velocity in the z-direction, $m.s^{-1}$
W dimensionless velocity in the z-direction
α thermal diffusivity, $m^2.s^{-1}$
β thermal expansion coefficient, K^{-1}
φ dimensionless electric potential,
θ dimensionless temperature
ρ density of the fluid, $kg.m^{-3}$
σ electrical conductivity, $\Omega^{-1}.m^{-1}$
υ kinematic viscosity of the fluid, $m^2.s^{-1}$
Plane PT or plane (y-z)Plane PV or plane (x-y)
Plane PH or plane (x-z) Lines CC mid-plane (x-y)
Lines AA mid-plane (x-z) LinesBBmid-plane(y-z)

Geometry and mathematical model

The geometry of the flow field analyses in this study is illustrated in Fig. 1. A liquid metal with a density ρ, a kinematics viscosity ν and an electrical conductivity σ, fills a rectangular cavity of dimensions $L \times H \times l$, having an aspect ratio $A=L/H=1$, and subjected to a uniform magnetic field B_0. The magnetic field is applied in the *y direction*. The cavity is isothermally heated from the left vertical wall with a uniform constant temperature T_H and the right vertical with temperature T_C ($T_H > T_C$). The fluid contained in the rectangular cavity is Galium whose Prandtl number equals to 0.019. We will refer to different cross-sections of the cavity, in order to describe both the numerical and the experimental flows.

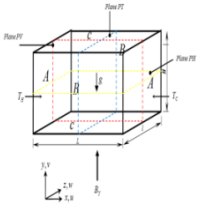

Figure 1. The geometry of the problem

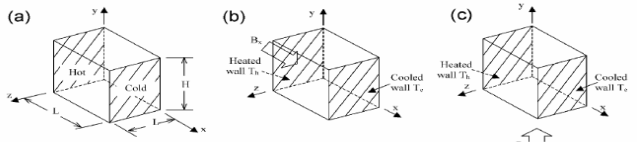

Figure 2. (a) Schematic diagram of the enclosure and coordinate system: uniform magnetic field in (b) x-, (c) y-directions.

We denote by (*X-Y)* Plane PV, (*Y-Z)* Plane PT and (*X-Z)* Plane HP cross sections, the planes which are perpendicular to the *z*, *x* and *y*-axes respectively and in addition, we indicate the coordinates of their centers.

Examples of three cross sections, centered on $x = Ax=1/2$, $y = 0$ and $z = 0$ can be seen in figure 1. These will commonly be referred to as the central cross-sections.

The governing equations are obtained using the following assumptions:

- Joule heating is negligible.
- Viscous dissipation is negligible.
- The induced magnetic field is negligible because $R_{em}<<1$.
- The liquid metal is not magnetized ($\mu_m=1$).
- The liquid metal is incompressible and Newtonian.
- The Boussinesq approximation holds.

The interaction between the magnetic field and convective flow involves an induced electric current

$\vec{j}: \vec{j} = \sigma\left[-\vec{\nabla}\varphi + \vec{V} * \vec{B}\right]$

The divergence of Ohm's law $\overrightarrow{\nabla . j} = 0$ produces the equation of the electric potential:

$$\nabla^2\varphi = \vec{\nabla}\left(\vec{V} \wedge \overrightarrow{e_B}\right) \quad (1)$$

Whereas those of F are obtained using the equation:

$\vec{F} = \vec{j}^* * \vec{B}$

By neglecting the induced magnetic field, the dissipation and Joule heating, and the Bousinesq approximation is valid; and using H, α/H, H^2/α, $\rho_0 (\alpha / H)^2$, αB_0 and $(T_H - T_C)$ as typical scales for lengths, velocities, time, pressure, potential, and temperature, respectively, the dimensionless governing equations for the conservation of mass, momentum ,and energy, together with appropriate boundary conditions in the Cartesian coordinates system *(x, y, z)*, are written as follows:

$$\nabla . V = 0 \quad (2)$$

$$\frac{\partial V}{\partial t} + (V.\nabla)V = -\frac{1}{\rho}\nabla p + \upsilon\nabla^2 V + g\,\beta(T - T_0)e_y + F \quad (3)$$

$$\frac{\partial T}{\partial t} + (V.\nabla)T = \alpha\nabla^2 T \quad (4)$$

where $Ra = \frac{g\beta(T_H - T_C)H^3}{\alpha\nu}$ are the Rayleigh number, $Gr = g\,\beta\left(T_H - T_C\right)\,H^3/\alpha^2$ is the Grashof number, $Ha = B_0\,H\sqrt{\sigma/\rho\upsilon}$ the Hartmann number, and $\Pr = \upsilon/\alpha$ the Prandtl number.

- Electric potential equation:

Horizontally applied magnetic field:

$$\frac{\partial^2\varphi}{\partial X^2} + \frac{\partial^2\varphi}{\partial Y^2} + \frac{\partial^2\varphi}{\partial Z^2} = \left[\frac{\partial W}{\partial Y} - \frac{\partial V}{\partial Z}\right] \quad (5\text{-a})$$

Vertically applied magnetic field:

$$\frac{\partial^2\varphi}{\partial X^2} + \frac{\partial^2\varphi}{\partial Y^2} + \frac{\partial^2\varphi}{\partial Z^2} = \left[\frac{\partial U}{\partial Z} - \frac{\partial W}{\partial X}\right] \quad (5\text{-b})$$

Transversally applied magnetic field: $\frac{\partial^2\varphi}{\partial X^2} + \frac{\partial^2\varphi}{\partial Y^2} + \frac{\partial^2\varphi}{\partial Z^2} = \left[\frac{\partial V}{\partial X} - \frac{\partial U}{\partial Y}\right]$ (5-c)

Case of a horizontal magnetic field when *B* is applied in the *x-direction*, the expressions are:

$F_X = 0$; $F_Y = \left(-\frac{\partial\varphi}{\partial Z} - V\right).Ha^2.Pr$; $F_Z = \left(\frac{\partial\varphi}{\partial Y} - W\right).Ha^2.Pr$; $j_X = -\frac{\partial\varphi}{\partial X}$ $j_Z = -\frac{\partial\varphi}{\partial Z} - V$ $j_Y = -\frac{\partial\varphi}{\partial Y} + W$

Case of a vertical magnetic field when B is applied in the *y-direction*, the expressions are:

$F_X = \left(\frac{\partial\varphi}{\partial Z} - U\right).Ha^2.Pr$; $F_Y = 0$; $F_Z = \left(-\frac{\partial\varphi}{\partial Y} - W\right).Ha^2.Pr$ $j_X = -\frac{\partial\varphi}{\partial Y} - W$ $j_Y = -\frac{\partial\varphi}{\partial Y}$ $j_Z = -\frac{\partial\varphi}{\partial Z} + U$

Case of a transversal magnetic field when B is applied in the z-direction, the expressions are:

$F_X = \left(-\frac{\partial\varphi}{\partial Y} - U\right).Ha^2.Pr$; $F_Y = \left(\frac{\partial\varphi}{\partial X} - V\right).Ha^2.Pr$; $F_Z = 0$; $j_Y = -\frac{\partial\varphi}{\partial Y} + V$ $j_Y = -\frac{\partial\varphi}{\partial Y} - U$ $j_Z = -\frac{\partial\varphi}{\partial Z}$

At $X = 0$; $U = V = W = 0$, $\Theta = 1$ *and* $\partial\varphi/\partial x = 0$

At $X = 4$; $U = V = W = 0$, $\Theta = 0$ *and* $\partial\varphi/\partial x = 0$

At $Y = 0$; $U = V = W = 0$, $\partial\Theta/\partial Y = 0$ *and* $\partial\varphi/\partial y = 0$

At Y = 1; U = V = W = 0, $\partial\Theta/\partial Y = 0$ and $\partial\varphi/\partial y = 0$

At Z = 0; U = V = W = 0, $\partial\Theta/\partial Z = 0$ and $\partial\varphi/\partial z = 0$

At Z = 1; U = V = W = 0, $\partial\Theta/\partial Z = 0$ and $\partial\varphi/\partial z = 0$

Numerical method

Equations (1-4) with the boundary conditions are solved by using the finite volume method [9]. Scalar quantities (*P, T, ϕ*) are stored in the center of these volumes, whereas the vectorial quantities (*u*, *v*, and *w*) are stored on the faces. For the discretisation of spatial terms, a second-order central difference scheme is used for the diffusion and convection parts of the equations (2-5), and the SIMPLER algorithm [9] is used to determine the pressure from continuity equation.

In MHD flows boundary layers different to those in ordinary hydrodynamics occur. At walls perpendicular to the magnetic field Hartmann layers of thickness $\delta_H \sim Ha^{-1}$ appear which are characterized by an exponential decay of the velocity towards the wall.

At walls parallel to the magnetic field, the so-called side layer exists, which is different in shape and thickness ($\delta_S \sim Ha^{-1/2}$) compared to the Hartmann layers. In order to capture the Hartmann and side layers and by taking into account the fact that their thickness diminishes as Ha increases ($\delta_H \sim Ha^{-1}$and $\delta_S \sim Ha^{-1/2}$) the grid line densities are chosen according to the value of the magnetic field *B* and its direction. These are given in Table 1. The increments *DX, DY* and *DZ* of the grid used are not regular. They are chosen according to geometric progressions of ratio 1.07 which permitted grid refinement near the walls; i.e. in the Hartmann and side layers where large velocity and temperature gradients exist, thus requiring a larger number of nodes.

Table 1 Meshes used in the computations

	Ha	Mesh size $N_x x N_y x N_z$
No magnetic field	**0**	**112x112x120**
y-Direction magnetic field fig.2 (b)	**25**	**112x112x120**
	50	**112x112x120**
	75	**112x112x120**
	100	**112x112x120**

The magnetic field direction ***y*** was resolved by a comparatively smaller number of points since the above-mentioned integral model was adopted for the Hartmann layers. Some simulations with no MHD effects were also performed; for these cases, a non-equispaced grid with $\mathbf{N_x x N_y x N_z}$= 112x112x120= 1404928 nodes was used Fig.3 (b). 10000 iterations at most were needed for a complete convergence of all variables; the convergence speed was thus higher than for the quasi-2D, fully developed, problem and was only slightly affected by the conductivity of the walls, the Rayleigh number, or the Hartmann number.

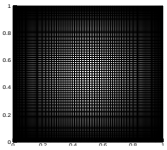

Figure 3. Mesh size, $N_x x N_y x N_z$

Computed results and discussion

Code validation

An important step in code development is to validate and compare the results computed from the code developed with published data from other computational codes.

The results at $Ra = 1.59.10^7$ and Ha=*10* computed by code development for two-dimensional and A=4 flow shown in Fig. 2. The stream functions and isotherms are in good agreement with the results of Gelfgat et al [7].

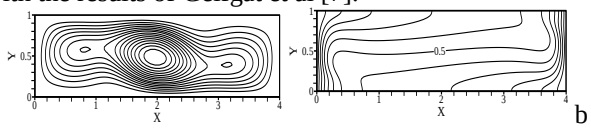

a b

Figure 3.For two-dimensional flow at $Ra = 1.59.10^7$, *Pr* = 0.019 and *Ha =10*: (a) stream functions ; and (b) isotherms .

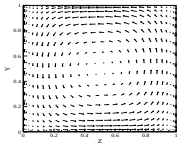

Figure 4. Current path for Ha= 25 in plane PT.

In order to give better insight into the physics behind the change in flow pattern, sketches of the cur-rent path in plane PT corresponding to Ha= 25 are given, respectively, in Fig. 3. The Lorentz forces are produced by the interaction between these currents and the applied vertical field. As can be noticed, the flowing fluid generates under the action of the magnetic field, currents which are positive in the neighborhood of the top wall and negative in the neighborhood of the bottom wall. This difference in sign is due to the different directions of the fluid in contact with the top and bottom walls. Because of this difference in sign, the Lorentz force acting on the top layers of the fluid is negative (i.e. a retarding force) and that acting on the bottom layers is positive (i.e. also a retarding force since the fluid flows in the negative direction towards the plane X= 0). The conservation equations of mass, momentum and energy are solved by Patankar's [9] SIMPLE algorithm with hybrid difference scheme.

The temperature is constant on horizontal lines in the layer of the central part. The temperature gradients are concentrated in two layers adjacent to the heated and the cooled walls, and the distortion of the temperature field near the corners, however, can be attributed to convective energy transport. This behavior of the temperature field can be interpreted as two thermal boundary layers on both vertical surfaces separated by a core with a temperature which is constant along horizontal lines but not along vertical lines.

The velocity vectors in vertical plane *x–y* are represented in Fig. 4 at three different levels of cavity depth, at quarter, mid and third planes. The velocity vectors of Fig. 4 indicate that the recirculation flow is adjacent to the walls, the central core of fluid is practically stagnant and the velocity maximum value moves closer to the wall as the Rayleigh numbers increase. Small change occurs in velocity values and flow patterns at *x–y* plane for the three different levels. This may be due to the effect of *w-velocity*, which is small.

The velocity vectors in the horizontal plane *x–z* are represented in Fig. 5. One can show that the w-velocity values are very small compared to those of *u* and *v* especially at $y = ¼$ and $¾$ *H*.

In effect, results obtained show that the flow and the thermal fields illustrated in the Figs. 5 a,b,c respectively relatively intense straining of the fluid for large values of *Gr*. We note the evolution of the stream function by increasing the *Gr* number.

Fig. 5c. Then, one notices light modifications which appear by increasing *Gr*. For $Gr=10^7$, small recirculation zones, also called "vortices". The thermal field of the flow is presented in Figs. 6, It should be noted that for a weak *Gr* number, no good stratification of the isotherms with the horizontal walls of the enclosure is observed. Indeed when the *Gr* number increases, we notice the presence of significant variations in temperature. This is explained by the existence of convective transport dominating the flow (the acceleration of the particles cause this phenomenon). The convection flow along the two adiabatic vertical walls shows the beginning of the development of a multi-cell flow within the cavity, which enhances effectiveness of heat transfer through top wall. This effect has been observed until Gr = 10^7, where the cross temperature gradient and the resulting multi-cell flow have become strong enough for heat transfer to be enhanced from the bottom wall to the top wall. In Fig. 7, we present the distribution of the velocity vectors. We notice, that for a small *Gr* value, the flow generates very weak velocity gradients, whereas when the Gr number increases, the flow induced by the increasing buoyancy forces, the flow becomes animated. Significant velocity gradients are then localized near the walls, resulting in the production of vortices.

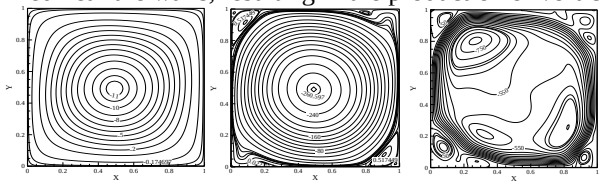

a b c

Figure 5. Structure of the flow represented contours of stream function by:Pr= 0.019; Ha=0 ; A=1; α=0, and for various Grashof number : a)- Gr=10^3 ; b)- Gr=10^5 ; c)- Gr=10^7.

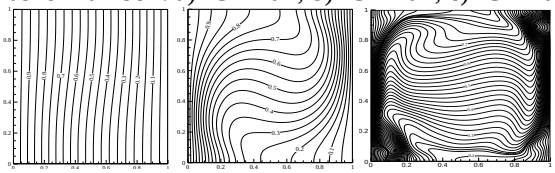

a b c

Figure 6. Structure of the flow represented isothermal by:Pr= 0.019; Ha=0 ; A=1; α=0, and for various Grashof number : a)- Gr=10^3 ; b)- Gr=10^5 ; c)- Gr=10^7

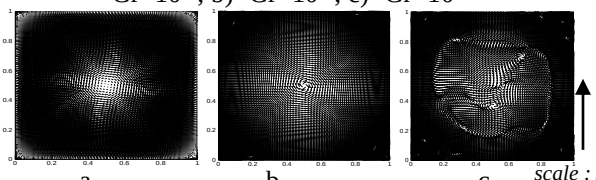

a b c

Figure 7. Structure of the flow represented by velocity vectors: Pr= 0.019; Ha=0 ; A=1; α=0, and for various Grashof number : a)- Gr=10^3 ; b)- Gr=10^5 ; c)- Gr=10^7.

Effects of the Hartmann Number

Figure 8 and Fig. 18 show the effect of the magnetic field in the two directions X and Y using different values of the Hartmann number (Ha = 0, 10, 50, 100).

We notice the results of the dynamic field presented, in the form of contours of the stream function, Fig. 8. The figures show that for Ha=10, the flow is characterized by many cells.
When the intensity of the magnetic field in the X direction increases, the number of cells reduces to two cells. On the other hand, in the Y direction, with the same intensities, the flow structure changes.

For Ha = 100, the cells begin to lose their organized shape. When Ha is increased further, the flow becomes unstable and a somewhat perturbed cell is apparent.

The effect of the magnetic field is significant when α equals 90^0. It is also noted that when the magnetic field is applied in the *Y* direction, the natural convection is clearly weakened. An elimination of the thermal stratification is obtained by increasing the *Gr* number. However, an increase in the intensity of the magnetic field leads to isotherms nearly parallel to the horizontal walls explaining the elimination of the convective phenomena and the presence of the conductive phenomena. This also explains the decelleration of the thermal transfer as confirmed by the average Nusselt number Fig. 13. Concerning the horizontal and vertical normalized velocity profiles, they are shown in Figs14 and 15 (in the case of the *X* direction magnetic field and *Y*-direction magnetic field) respectively.
It is clear from the results that as *Ha* increases; the velocity components tend to decrease. In fact, for *Ha*=120, their values are practically equal to zero in the major part of the cavity except near the end walls. It is thus clear that the use of a magnetic field can strongly decrease the flow intensity, but cannot completely inhibit fluid motion.

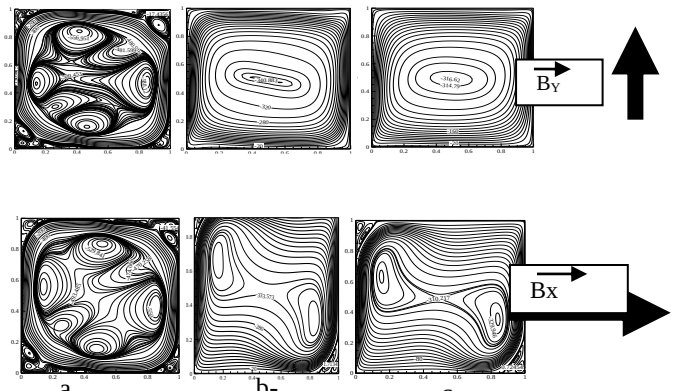

Figure 8. Structure of the flow represented by contours of stream function, for: $G_t=10^7$, *A=1*, *Pr*=0.019, and for various Hartmann number: *a- Ha=30; b- Ha=100; c- Ha=120*. Avec : 1-α= 0, 2-α=90˚.

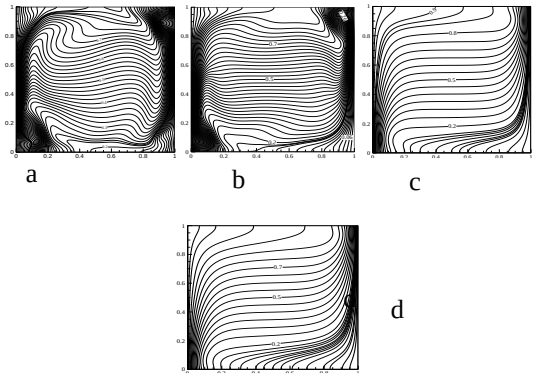

Figure 9. Structure of the flow represented by isothermal, for: $G_t=10^7$, *A=1*, *Pr*=0.019, and for various Hartmann number: *a)-Ha=0; b)-Ha=30; c)-Ha=100; d)-Ha=120*. with : -α=90˚.

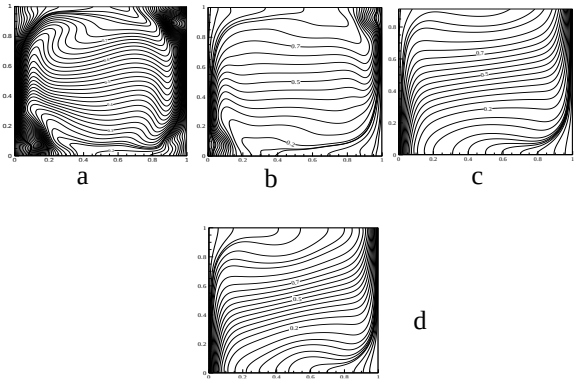

Figure 10. Structure of the flow represented by isothermal, for: $G_t=10^7$, *A=1*, *Pr*=0.019, and for various Hartmann number: *a)-Ha=0; b)-Ha=30; c)-Ha=100; d)-Ha=120*. with : -α=0˚.

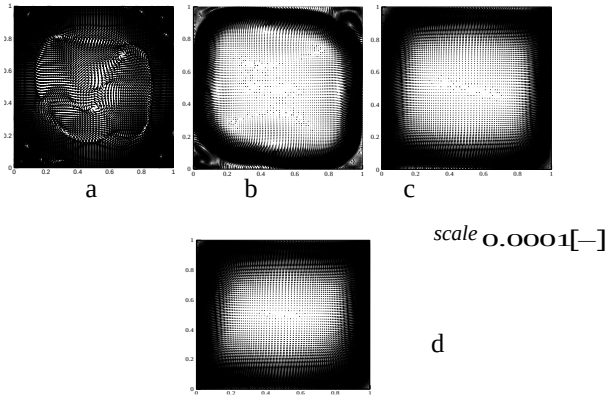

Figure 11. Structure of the flow represented by velocity vectors, for: $G_t=10^7$, *A=1*, *Pr*=0.019, and for various Hartmann number: *a)-Ha=0; b)-Ha=30; c)-Ha=100; d)-Ha=120*. with : -α=90˚.

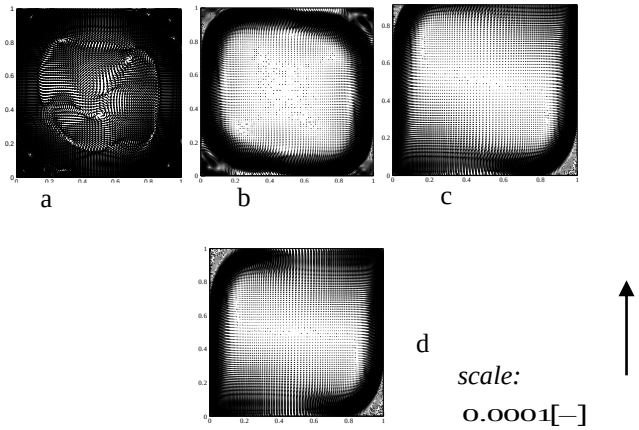

Figure 12. Structure of the flow represented by velocity vectors, for: $G_t=10^7$, $A=1$, $Pr=0.019$, and for various Hartmann number: *a)-Ha=0; b)-Ha=30; c)-Ha=100; d)-Ha=120*. with : $\alpha=0^\circ$.

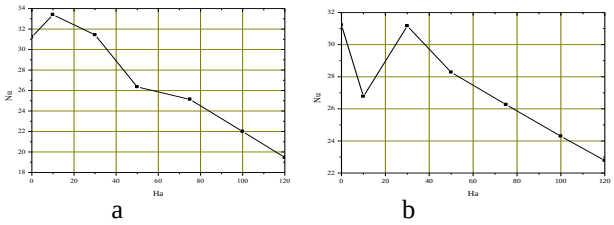

Figure 13. Variation the average Nusselt number according to *Ha -a)* directions X. *–b)* directions Y

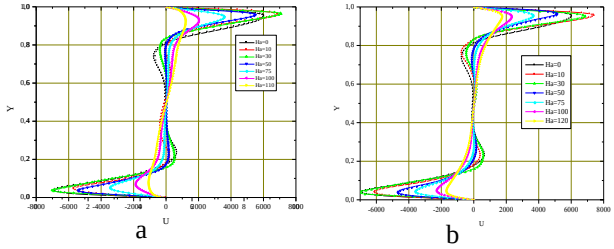

Figure 14. Profiles of horizontal velocity component at x=1/2, -a) *a)* directions *X*. *–b)* directions *Y*

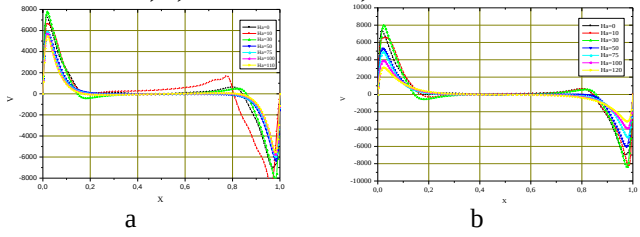

Figure 15. Profiles of vertical velocity component at Y=0.5, -a) *a)* directions *X*. *–b)* directions *Y*

Effect of wall conductivity

Figs. 16(a, b and c) show that for insulated walls the surface representing the distribution of electric potential, presents variations less important than those corresponding to conducting walls. These high gradients in electric potential in the case of conducting walls are reflected, according to Ohm's law in higher values of the electric current (Figs. 17 case1 and case4) and hence in those of the Lorentz force. Wall electrical conducting leads therefore to lower source or to higher sink terms in the momentum equations, depending on the flow direction; i.e. to an overall damping of the flow. This can be noticed through the comparison of the maximum velocities shown in Fig. 16(a). Another way for viewing the effect of magnetic field is to use the Lycoudis number Ly [3] defined by $Ly=2Ha^2/Ra^{½}$ and traditionally employed to correlate the heat transfer rate of free convection of a liquid metal in an external magnetic field. The above conclusions that the convection is deadened more effectively when the frontal walls (Z=0 and Z=1) are electrically conducting. This is due to the fact that the walls electrically conducting lead to a weak source or terms raised in the equations of momentum depend on the direction of the flow, with a complete damping of the flow For example, with (Ha=10) the average Nusselt number is (2.5) without unit for case 1 is (1.4) without unit for case 4 Fig. 17.

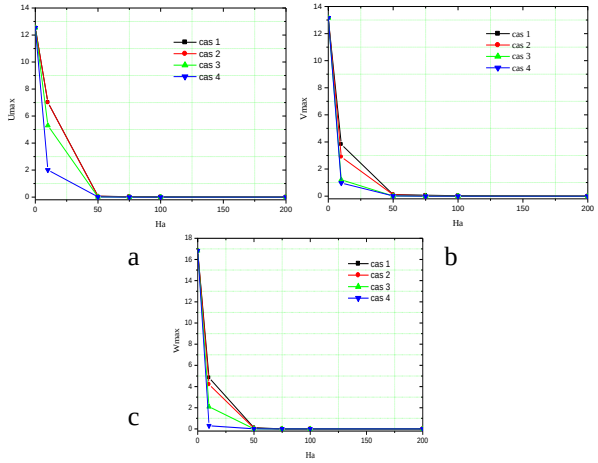

Figure 16. Variation of umax, vmax, and wmax with the Hartmann number for the various cases (***case 1***: all the walls are electrically insulating; case ***2***: only the vertical walls are electrically conducting; case ***3***: only the horizontal walls are electrically conducting; case ***4***: only the frontal walls are electrically conducting) **(a)** umax, **(b)** vmax, **(c)** wmax.

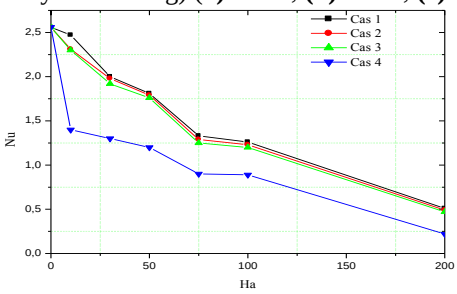

Figure 17. Variation of average Nusselt number Nmoy with the Hartmann number Ha and various cases (***case 1:*** all the walls are electrically insulating; case ***2:*** only the vertical walls are electrically conducting; case ***3:*** only the horizontal walls are electrically conducting; case ***4:*** only the frontal walls are electrically conducting), for $Gr=10^7$.

Conclusion

A numerical study was carried out for the effect of *x, y* and *z-direction* uniform magnetic field on three-dimensional flow and temperature distribution of molten Galium natural convection

in an enclosed cavity heated from one vertical wall and cooled from an opposing vertical wall. The results show that the *y-direction* external magnetic field was found to be the most effective in suppressing convection, and the *y-direction* field to be the least effective at Ha = 120 with reduction in Nusselt number value. The average Nusselt number values decrease with increase in Hartmann number values. Also, electrical wall conductivity changes the Lorentz force distribution by increasing it in regions where it opposes the flow, decreasing it in the remaining regions where it is favorable to the flow: the consequence being an enhanced damping of the flow.

In conclusion, the results indicate that one can control the flow via a good choice of the strength and direction of the magnetic field, as well as of the electric conductivity of the cavity walls.

References

[1] Carrie F., Proust E., Remolouv J., Racaboy A., Tilliette Z., Fusion reactor blanket – comparative evaluation study, Report *EMT/SERMA/BP/84/No*. 584 T, 3591-21-000, 1984.

[2] Hill P. 1998 Crystal growth meets demands of opto devices. *Opto & Laser Europe* **56**, 33{35.

[3] Muller G. & Ostrogorsky A. 1993 Convection in melt growth. *Handbook of Crystal Growth*, vol. 2b (ed.) D. T. J. Hurle. North-Holland.

[4] Tagawa T., Ozoe H., " Enhancement of heat transfer rate by application of a static magnetic field during natural convection of liquid metal in a cube" *ASME Journal of Heat Transfer vol.* 119, 1997, pp. 265-271.

[5] Benhadid H., Henry D., "Numerical study of convection in the horizontal Bridgman configuration under the action of a constant magnetic field. Part2. Three-dimensional flow" *Journal of Fluid Mechanics vol.* 333, 1997, pp. 57-83.

[6] Bessaih R., Kadja M., Marty Ph., "Effect of wall electrical conductivity and magnetic field orientation on liquid metal flow in a geometry similar to the horizontal Bridgman configuration for crystal growth" *International Journal of Heat and Mass Transfer vol. 42*, 1999, pp. 4345-4362.

[7] Kherief N M., Talbi K.and Berrahil F. Effects of Inclination and Magnetic Field on Natural Convection Flow Induced by a Vertical Temperature. *Journal of Applied Fluid Mechanics 5(1),* 113-1 202012.

[8] Kherief, N M., K. Talbi and F. Berrahil. Magneto-Hydrodynamic Flow in a Two-Dimensional Inclined Rectangular Enclosure Heated and Cooled on Adjacent Walls. *Journal of Applied Fluid Mechanics* Vol. 9, No. 1, pp. 205-213, 2016.

[9] Patankar S.V. [1980] Numerical Heat Transfer and Fluid Flow. Hemisphere: Washinton DC, ch.4